Symmetry Breaking of Graphene Monolayers by Molecular Decoration

Xiaochen Dong,[1,4] Yumeng Shi,[1] Yang Zhao,[1] Dongmeng Chen,[1] Jun Ye,[1] Yugui Yao,[5] Fang Gao,[1] Zhenhua Ni,[2] Ting Yu,[2] Zexiang Shen,[2] Yinxi Huang,[3] Peng Chen,[3,*] and Lain-Jong Li[1,*]

[1]*School of Materials Science and Engineering, Nanyang Technological University, Singapore*
[2]*School of Physical and Mathematical Sciences, Nanyang Technological University, Singapore*
[3]*School of Chemical and Biomedical Engineering, Nanyang Technological University, Singapore*
[4]*Institute of Advanced Materials, Nanjing University of Posts and Telecommunications, Nanjing, China*
[5]*Institute of Physics, Chinese Academy of Sciences, Beijing 100190, China*
(Received 14 October 2008; published 31 March 2009)

Aromatic molecules can effectively exfoliate graphite into graphene monolayers, and the resulting graphene monolayers sandwiched by the aromatic molecules exhibit a pronounced Raman G-band splitting, similar to that observed in single-walled carbon nanotubes. Raman measurements and calculations based on the force-constant model demonstrate that the absorbed aromatic molecules are responsible for the G-band splitting by removing the energy degeneracy of in-plane longitudinal and transverse optical phonons at the Γ point.

The existence of monolayered graphene was discovered very recently through mechanical exfoliation of graphite [1]. Its unique electrical, physical, and optical properties promise a variety of fundamental studies and applications [2,3]. Here, we show that aromatic molecule tetrasodium 1,3,6,8-pyrenetetrasulfonic acid (TPA) can effectively exfoliate graphite into graphene monolayers with the aid of sonication in aqueous solutions. Almost 90% of the graphene sheets dispersed on SiO_2 substrates are identified as monolayered. Normally, only a single G peak (1580 up to 1590 cm^{-1}) is present in the Raman spectrum of pristine graphene [4] due to energy degeneracy of two optical phonon modes (LO and TO) at the Γ point [5,6]. Interestingly, it is found here that the Raman G-band of the aromatic molecule-dispersed graphene monolayer is split into two distinct peaks. We note that such unambiguous G-band splitting has only been observed in single-walled carbon nanotubes because of symmetry breaking related to rolling up of graphene monolayers. We further demonstrate that interactions between aromatic molecules and the graphene monolayers can induce G-band splitting by lifting the two-fold degeneracy of LO and TO phonons. This notion is corroborated by symmetry-based force-constant-model calculations considering up to 4th-nearest-neighbor interactions.

In a typical experiment for dispersing graphenes by TPA molecules, 1 mg of graphite powders (NGS, Germany) mixed with 10–20 mg of TPA were sonicated in 5 ml D_2O solution using a probe sonicator (pulse mode in an ice bath with 70 W for ~2 hr). After gravity sedimentation for overnight, the resulting supernatant was then drop casted onto 300 nm of thermal oxide on a Si substrate, followed by rinsing using deionized water. Raman spectra were measured in a WITec CRM200 confocal Raman microscopy system equipped with three lasers (457, 488, and 532 nm), and the Si peak at 520 cm^{-1} was used as a reference for wave number calibration.

Figure 1(a) presents a typical atomic force microscopy (AFM) image of graphene layers drop casted on the SiO_2 substrate. Thirty-four pieces of graphene sheets are found in a 10 μm $\times$ 10 μm area, while the sizes of these graphene patches are around 100–500 nm. The cross section profiling across the highlighted area is shown in a magnified scale [Fig. 1(a), right], indicating a thickness of gra-
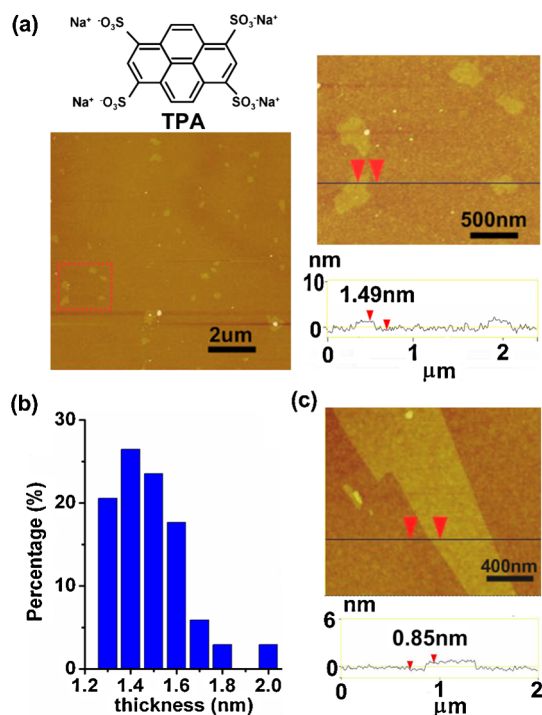

FIG. 1 (color online). (a) A typical AFM image of graphene sheets dispersed in TPA/D_2O solution and subsequently drop casted on a SiO_2 substrate. (b) The thickness distribution of all the graphene sheets observed in (a). (c) AFM image of a mechanically exfoliated HOPG monolayer.

phene sheet of ~1.5 nm. Thirty out of all 34 observed graphene sheets in Fig. 1(a) (left) are 1.29 to 1.65 nm thick. As depicted in Fig. 1(b), the thickness is narrowly distributed with a mean of ~1.49 nm. The measurements, however, include the contribution from adsorbed TPA molecules. To benchmark with the thickness of the pure graphene monolayer, parallel AFM measurements were performed on the mechanically exfoliated graphene monolayers from highly oriented pyrolytic graphite (HOPG), from which a thickness of ~0.85 nm is observed [Fig. 1(c)]. It is noted that the measured thickness 0.85 nm for monolayers is reasonable because the documented values of monolayer thickness vary from 0.4 to 1.2 nm due to instrumental offset [7]. Assuming that TPA molecules are covering both sides of the graphene monolayer through face-to-face interaction and the distance between TPA and graphene is ~0.35 nm [8], the mean thickness obtained in Fig. 1(b) corresponds to a mean graphene thickness of ~0.8 nm, in good agreement with the measurement on mechanically scratched bare graphene monolayers. The variation in AFM measurements is attributable to the inhomogeneous coverage of TPA molecules and system noises. One particular sample, which is exceptionally thick (2.2 nm), is likely a graphene multilayer. These results convincingly demonstrate the effectiveness of our method in exfoliating graphite into graphene monolayers.

The characteristic G (~1600 cm^{-1}) and 2D (~2700 cm^{-1}) bands depend on the number of stacked graphene layers [7,9–11] and are often sensitive to the presence of impurities or surface charges [12]. Figure 2(a) shows the Raman G and 2D spectra for TPA-dispersed graphene monolayers, and those for TPA-dipersed graphene multilayers (2.4 nm thick from our AFM; indicated as ML) with mechanically exfoliated HOPG monolayers (HOPG1L) included as a comparison. A single G-band at 1585 cm^{-1} and a 2D band at 2696 cm^{-1} (peak width ~26 cm^{-1}) are observed for HOPG1L, consistent with those previously reported [7,9]. In contrast to the Raman spectra from HOPG1L, two distinct G-band peaks at ~1567 and 1591 cm^{-1} are observed from the TPA-dispersed graphene monolayers, as demonstrated in Fig. 2(a). We note that the G-band splitting is unlikely due to residual TPA molecules themselves because those adsorbed on graphite or multilayer graphene are not able to produce the splitting. In addition, excess TPA molecules are removed by a rigorous washing procedure until all characteristic Raman peaks from the TPA molecules disappear. On the other hand, an apparent correlation between Raman and AFM measurements is observed. Specifically, the G-band splitting and the relatively sharp 2D band are only observed from the graphene sheets thinner than 1.65 nm. If the thickness exceeds 2 nm, only a single G peak and a widened 2D peak (with a width ~79 cm^{-1}) are observed. Natural graphite normally adopts AB-stacking sequence , and since the Raman 2D bandwidth has been suggested to distinguish between
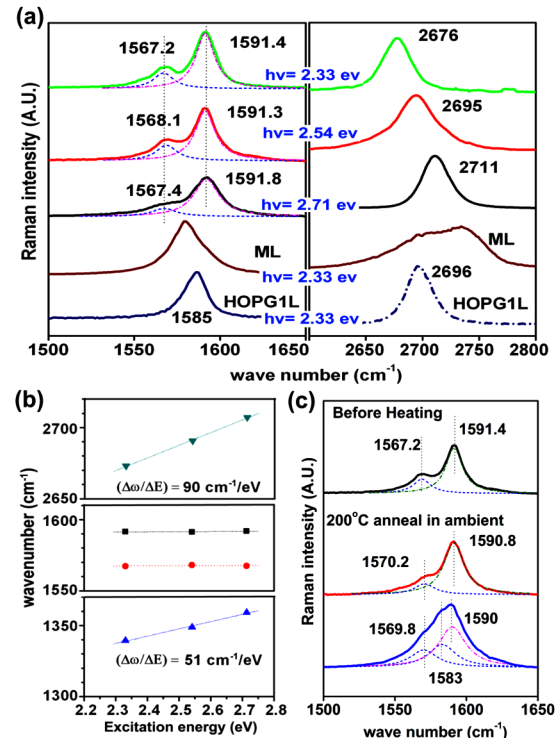

FIG. 2 (color online). (a) Raman G and 2D spectra of the TPA-dispersed graphene monolayer (excited by three laser energies 2.33, 2.54, and 2.71 eV) and multilayer (ML). Raman spectrum for reference sample, mechanically exfoliated HOPG monolayer (HOPG1L) is also included. (b) Frequency-energy dispersion ($\Delta\omega/\Delta E$) of D, G, and 2D bands for TPA-dispersed graphene monolayers. (c) G bands for TPA-dispersed graphene monolayer before and after thermal treatment (200 °C in ambinet).

monolayered and multilayered AB-stacked graphene [14], we are able to examine a total of 73 sheets from 10 different locations on the sample using this method, and 65 sheets (~90%) are identified as monolayers. This fits well with the statistics (the content of monolayered graphene) from AFM measurements, which further confirms our assignments of the monolayered and multilayered graphene samples dispersed by TPA.

From Figs. 2(a) and 2(b), the G-band spectra from the same TPA-dispersed graphene monolayer excited at three different laser energies (2.33, 2.54, or 2.71 eV) can be fitted with two Lorentzians peaked at ~1567 and 1591 cm^{-1}. This excitation-energy independence is in line with a first-order Raman process. Furthermore, the observed sharp and intense G-band signal is much more likely originated from the first-order Raman process, which is a direct and deterministic phonon generation process, than 2nd-order double-resonance scattering, which produces phonons with a broad energy distribution due to defect scattering [15]. According to the first-order process, the presence of two distinct G peaks in TPA-dispersed graphene monolayers indicates that two phonon energies are allowed at the Γ point. It is believed that TPA alters the electron density distribution of the pristine graphene monolayer and hence

leads to phonon symmetry breaking at the Γ point (lifting degeneracy of LO and TO), which, in turn, splits the Raman G modes. Figure 2(c) shows the G bands for the TPA-dispersed graphene monolayer before (top panel) and after the thermal treatment at 200 °C in ambient for 50 min (middle and bottom panels). Two typical changes in Raman G bands were observed after thermal degradation: namely, (1) the G-band splitting was narrowed (middle panel), or (2) the pristine graphene peak became pronounced (bottom panel). These observations suggest that after thermal degradation of TPA molecules, the G-band splitting was significantly reduced.

On the other hand, emission of a phonon with an excitation-energy dependent wave vector q ($\neq 0$) is often explained by a double-resonance scattering process [16–18], in which an electron is scattered from one wave vector k state to another and then back to its original k state. In accordance with this theory, the Raman energy is not generated from phonons in the first-order process ($q \sim 0$); rather it varies with the excitation energy. Although the double-resonance scattering theory is not able to provide a straightforward interpretation for the G-band signals of graphite and graphene, it well explains the excitation-energy dependences of the D and $2D$ bands for TPA-dispersed graphene monolayers. Figure 2(b) shows that the frequency-energy dispersion $\Delta\omega/\Delta E$ of the D and $2D$ bands for the TPA-dispersed graphene monolayers is ~ 51 cm^{-1}/eV and ~ 90 cm^{-1}/eV, respectively, in good agreement with the values for graphite (51–60 cm^{-1}/eV for the D band [19,20] and ~ 106 cm^{-1}/eV for the $2D$ band [15]) and the prediction by the double-resonance scattering theory [16–18].

It has been shown that inclusion of up-to-4th-neighbor interaction terms in the force-constant model is sufficient to reproduce the Raman data for graphite [5,6]. To understand the mechanism underlying the G-band splitting, a symmetry-based force-constant model is used to calculate phonon dispersion relations. It is plausible that the pyrene backbone in TPA changes the electron density in the graphene layer and hence leads to symmetry breaking, which alters the Raman G modes. Such influences from the TPA molecules can be simulated by modifying the spring constants of pristine graphene for up to 4th nearest neighbors. And calculations are carried out by assuming that a graphene sheet is sandwiched by two parallel films of TPA molecules located at an equal distance from the sheet. Figure 3(a) presents the unit cell used in the calculations. In Fig. 3(b), only one TPA molecule is shown hovering over a graphene sheet for illustration. To confirm that these matrix elements break the 6-fold symmetry due to absorbed molecules, we have also calculated force-constant matrices for prototype sandwiched systems using DFT. First, a full geometry optimization is performed including the optimization of the lattice constants using the DMol3 package (with all electrons considered) and the GGA (PBE) and DNP basis sets. Once the optimized structure is obtained, the force constants are calculated directly by altering
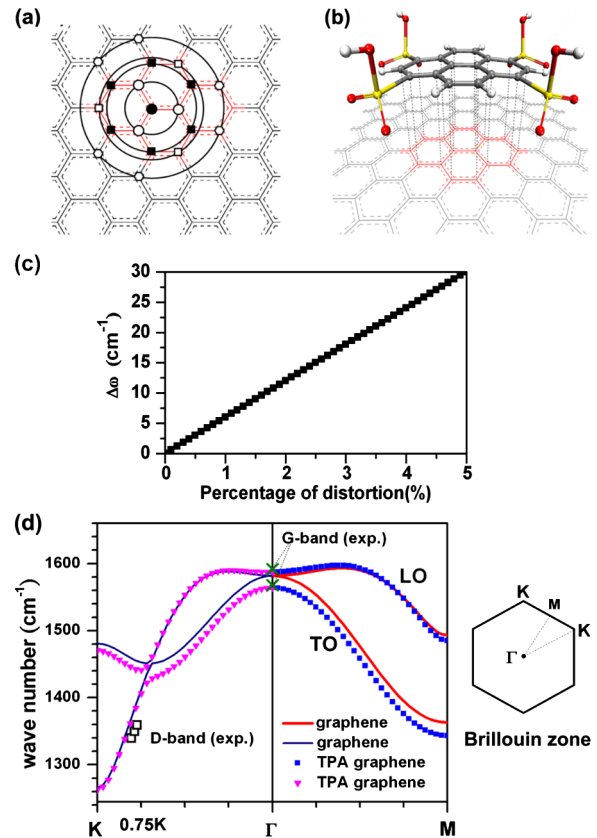

FIG. 3 (color online). Shown are (a) neighbor atoms on a graphitic plane up to 4th nearest neighbors of an A atom in a graphene unit cell (solid circle at the center). Open circles, solid squares, open squares, and open hexagons denote the 1st, 2nd, 3rd, and 4th nearest neighbor atoms, respectively. Portion of the hexagon lattice painted red labels the position of the pyrene backbone; (b) A TPA molecule over a graphene sheet with its vertical projection on the sheet. The TPA molecule is composed of a pyrene backbone and four sulfonate functional groups as shown in the plot. The grey spheres are carbon atoms of the pyrene backbone; (c) energy split of LO and TO phonons as a function of the percentage change in force constants; (d) calculated in-plane longitudinal and transverse (LO and TO) phonon dispersion relations of 2-dimensional graphene along the Γ to M directions for TPA-modified graphene. Two-dimensional Brillouin zone of graphene monolayers is also shown on the right.

atomic positions in both pristine and decorated graphene. Details will be addressed in a future publication [21]. Our DFT calculations conclude that absorbed aromatic molecules are able to induce spring-constant changes on up to 4th nearest neighbors breaking the 6-fold symmetry in the graphene sheet [21], and thus effectively split the twofold degeneracy of the optical phonon bands at the Γ point. This symmetry breaking is believed to be responsible for the observed G-band splitting. The energy split obtained from modified force constants is found to be linearly related to the percentage change of the force constants as shown in Fig. 3(c). According to this relation, the observed ~ 24 cm^{-1} splitting in Fig. 3(a) can be accounted for
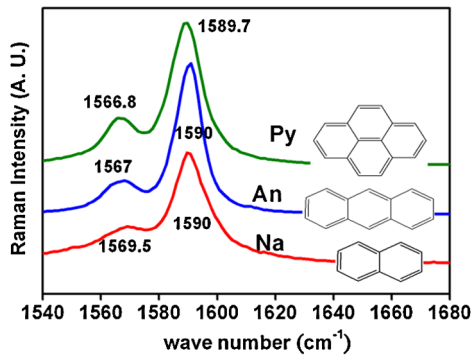
FIG. 4 (color online). Raman *G* band splitting observed in graphene monolayers dispersed by various aromatic molecules; naphthalene (Na), anthracene (An), and pyrene (Py).

when the force constants of TPA-dispersed graphene monolayer differ from that of pristine graphene monolayer by ~4%. In Fig. 3(c), LO and TO phonon dispersion relations of a 2-dimensional graphene sheet are plotted along the Γ-to-*M* and Γ-to-*K* directions, for both pristine graphene using documented force constants [5], and TPA-dispersed graphene monolayers with force constants differing from those of the pristine graphene by ~4%. The phonon dispersion curves for TPA-dispersed graphene sheets are similar in shape to those for pristine graphene except the symmetry breaking at the Γ point. In Fig. 3(d), the experimentally observed, excitation-energy dependent *D*-band frequencies (1339, 1350, 1359 cm^{-1}) are also depicted as open squares versus respective electronic wave vectors *k* (0.806, 0.788, 0.744 K). These *k* vectors correspond to the excitation energy used (2.33, 2.54, and 2.71 eV) [18]. Calculated curves are in good agreement with observed *D*-band frequencies [squares in Fig. 3(d)], implying that the *D* and 2D frequencies are not significantly affected by the aromatic decoration.

Similar *G*-band splitting is also observed in pyrene dispersed graphene monolayers (Fig. 4), but not in sodium dodecylbenzene sulfonate (SDBS) dispersed monolayers. Note that the SDBS exhibits the same ionic chains existed in TPA molecules. These results suggest that the *G*-band splitting is caused by the aromatic structure rather than the ionic side-chains of TPA. Figure 4 further demonstrates the *G*-band splitting induced by aromatic molecules with different ring sizes. It shows that larger aromatic rings such as anthracene and pyrene produce a wider split (~23 cm^{-1}) than smaller rings such as naphthalene (~20 cm^{-1}), presumably due to stronger interactions from larger aromatic rings. No graphene monolayers are found in suspension using the compounds with monoaromatic rings, such as benzene or toluene. It is likely that the interaction between monoring and graphene is not strong enough for graphite exfoliation. Furthermore, no *G*-band splitting is observed in the HOPG1L sheets drop casted with the all the four aromatic molecules used. We speculate that, in these cases, the influence from the molecules is weakened as the graphene layers unavoidably interact with the substrates, and

the molecules are only absorbed onto the top surface of the HOPG1L.

In summary, a high yield of monolayerd graphene sheets is achieved by exfoliation of graphite powders with TPA molecules. Observed *G*-band splitting in TPA-dispersed graphene monolayers is explained by lifting of the twofold degeneracy of the optical phonons at the Γ point. A direct consequence of the symmetry breaking is a modified electronic structure of the graphene sheet, which would induce band-gap opening therefore making possible a graphene device of a high on-off ratio. This study opens up an exciting possibility to tailor electronic structures of graphene by molecular decoration.

*ljli@ntu.edu.sg; ChenPeng@ntu.edu.sg

[1] K. S. Novoselov *et al.*, Science **306**, 666 (2004).
[2] F. Schedin *et al.*, Nature Mater. **6**, 652 (2007).
[3] H. B. Heersche, P. Jarillo-Herrero, J. B. Oostinga, L. M. K. Vandersypen, and A. F. Morpurgo, Nature (London) **446**, 56 (2007).
[4] C. Casiraghi, S. Pisana, K. S. Novoselov, A. K. Geim, and A. C. Ferrari, Appl. Phys. Lett. **91**, 233108 (2007).
[5] R. Saito, G. Dresselhaus, and M. S. Dresselhaus, *Physical Properties of Carbon Nanotubes* (Imperial College Press, London, 1998).
[6] M. S. Dresselhaus and P. C. Eklund, Adv. Phys. **49**, 705 (2000).
[7] A. Gupta, G. Chen, P. Joshi, S. Tadigadapa, and P. C. Eklund, Nano Lett. **6**, 2667 (2006).
[8] Y. Xu, H. Bai, G. Lu, C. Li, and G. Shi, J. Am. Chem. Soc. **130**, 5856 (2008).
[9] A. C. Ferrari *et al.*, Phys. Rev. Lett. **97**, 187401 (2006).
[10] Z. H. Ni *et al.*, Nano Lett. **7**, 2758 (2007).
[11] D. Graf *et al.*, Nano Lett. **7**, 238 (2007).
[12] I. Calizo, W. Bao, F. Miao, C. N. Lau, and A. A. Balandin, Appl. Phys. Lett. **91**, 201904 (2007).
[13] J. C. Charlier, X. Gonze, and J.-P. Michenau, Carbon **32**, 289 (1994).
[14] A. Das *et al.*, Nature Nanotech. **3**, 210 (2008).
[15] R. Sato *et al.*, New J. Phys. **5**, 157 (2003).
[16] J. Maultzsch, S. Reich, and C. Thomsen, Phys. Rev. B **64**, 121407(R) (2001).
[17] J. Maultzsch, S. Reich, U. Schlecht, and C. Thomsen, Phys. Rev. Lett. **91**, 087402 (2003).
[18] S. Reich, C. Thomsen, and J. Maultzsch, *Carbon Nanotubes-basic Concepts and Physical Properties* (Wiley-VCH, Weinheim, 2004).
[19] C. Thomsen and S. Reich, Phys. Rev. Lett. **85**, 5214 (2000).
[20] M. J. Matthews, M. A. Pimenta, G. Dresselhaus, M. S. Dresselhaus, and M. Endo, Phys. Rev. B **59**, R6585 (1999).
[21] Y. Zhao *et al.* (to be published).